*-Nickel-Iron Spinel /Reduced Graphene Oxide Nanocomposites: Structural and Mossbauer Studies

Volodymyra Boychuk, Volodymyr Kotsyubynsky, Khrystyna Bandura, Sofia Fedorchenko
Vasyl Stefanyk Precarpathian National University
Ivano-Frankivsk, Ukraine
kotsuybynsky@gmail.com

***Abstract*— Ultrafine nickel ferrite and nickel ferrite/ reduced graphene oxide (rGO) nanocomposite have been synthesized by hydrothermal method. Structural and magnetic properties of the obtained materials have been studied. XRD studies revealed that the joint hydrothermal synthesis of nickel ferrite and graphene oxide reduction leads to decreasing of ferrite particles to 8-9 nm. Normalized pair distance distribution functions and the most probable particle sizes were studied by SAXS method. The distribution of Fe^{3+} and Ni^{2+} cations between tetrahedral and octahedral sublattices was analyzed and transitions magnetic ordered state – spin glass like state - superparamagnetic state for ultrafine nickel ferrite were observed by Mossbauer spectroscopy.**

Keywords – nickel ferrite; reduced graphene oxide; nanocomposite material; mossbauer spectroscopy; cation distribution

I. INTRODUCTION

Ultrafine ferrites with spinel structure due to successful combination of purposefully variable magnetic and electrical properties are used now in the field of optoelectronics and spintronics [1], biological applications (cancer hyperthermia therapy, magnetic resonance imaging, drug delivery) [2,3], catalyst and sorbent [4], as electrode materials for lithium power source and supercapacitors [5]. Among the wide range of spinel materials soft magnetic nickel ferrite $NiFe_2O_4$ with high chemical stability is perspective material for electrochemical applications, catalyst and biomedicine [6, 7]. The obtaining of composite materials on the base of nickel ferrite and carbon nanoctructures, especially graphene and reduced graphene oxide allows overcoming problem with low n-type electrical conductivity of pure ferrite with simultaneously saving and improving of electrochemical performance [8-10].

From this point of view the influence of simple and effective methods of $NiFe_2O_4$ / rGO obtaining with establishment of synthesis conditions on its structural, magnetic and morphological properties is important.

II. EXPERIMENTAL DETAILS

A. Preparation of GO, NIS, and NIS / rGO materials

GO was obtained using well-known Hammers method [11]. The reduction of GO was carrying out under the hydrothermal conditions with the using of hydrazine hydrate.

Ultrafine nickel-iron spinel (NIS) samples were synthesized by hydrothermal method. Nickel nitrate (1.164 g) and ferric nitrate (3.234 g) were dissolved in distilled water (120 ml) under stirring at room temperature for 25 minutes. Sodium hydroxide aqueous solution was added drop wise until pH is 10.0. The obtained sol was sealed into Teflon-lined stainless steel autoclave and heated at 180 ^oC for 10 hours. The obtained precipitate was separated and washed several times in distilled water to neutral pH. Finally it was dried at 60°C for up to mass stabilization to get the as-synthesized sample.

At the first stage of NIS / rGO composite material preparation GO sol (80 mg GO dispersed in 60 mL of distilled water via ultrasonication for 120 min) was added to aqueous solution of nickel nitrate and ferric nitrate with the next slow hydrazine hydrate adding and to adjust pH to 10.0 by 5M NaOH. Last stage of synthesis was performed similarly to carbon-free NIS preparation.

B. Materials characterization

The phase composition and structure of the synthesized materials were analyzed by XRD and SAXS on a DRON-3M powder diffractometer (Cu Kα radiation). The average size of coherent scattering domains (CSD) was calculated by Scherrer's formula. Morphological properties were investigated by low-temperature nitrogen absorption/ desorption (Quantachrome Autosorb Nova 2200e device). Mossbauer spectra were measured with moving absorber using MS1104Em spectrometer with 1.7×10^7 Bq ^{57}Co (Cr) radiation source. Calibration of the isomeric shift was made using α-Fe foil. The velocity resolution was ~0.006 mm/s per channel. The obtained signal-to-noise ratios were higher than 25. The Mossbauer spectra were measured at temperature range from 90 to 293 K in transmission geometry. Chemical composition of the obtained materials was investigated by X-ray fluorescence analysis (Expert 3L device, not less 0.01 mass %)

III. RESULTS AND DISCUSSION

Fig. 1 shows the X-ray diffraction patterns of rGO, hydrothermally synthesized NIS and NIS / rGO. The XRD pattern for rGO shows broad characteristic (002) diffraction peak at about $2\theta = 25^o$ [12]. XRD data for NIS sample corresponds to monophase cubic spinel (cubic, PDF 00-023-1119, a = 0.8367 nm). The average crystallite sizes of nickel-iron spinel phase were about 26 nm. The peak broadening for NIS / rGO XRD pattern was observed due to average particle sizes decreasing to about 8-9 nm.

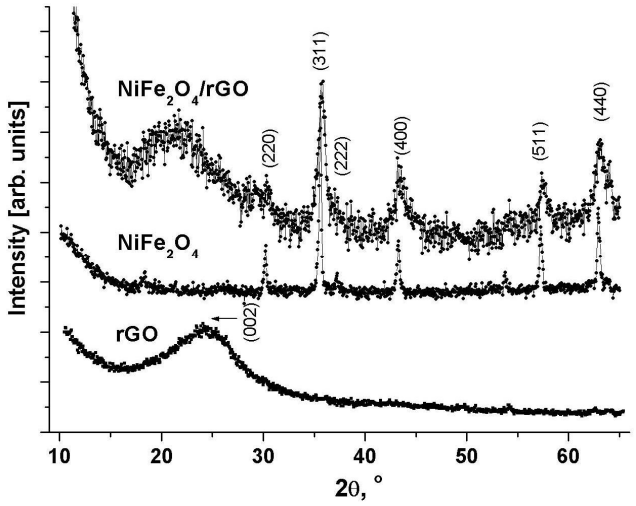

Fig. 1. XRD patterns of rGO, NIS and NIS / rGO samples

The wide halo in 2θ range of 15-27° is a result of amorphous rGO component presence. Basal reflection (002) peak for graphite is at 2θ=26.6° that corresponds to the interplanar distance of 3.35 Å. The shift of characteristic diffraction peak of rGO from about 2θ=24.7° for reduced graphene oxide sample to 2θ=22.5° corresponds to enlarging of average distance between graphene layers from 3.60 to 3.95 Å, respectively. The increasing of interplanar distance is an evidence of rGO sheets restacking and rearrangement after reduction carried out simultaneously with the NIS nucleation when the anchoring of spinel nanoparticles on the rGO fragments is possible. The specific surface areas were 40 and 150 m^2 / g for NIS and NIS / rGO, respectively.

Structural arrangement of the obtained materials was investigated by X-ray small-angle scattering (SAXS). The experimental plots of X-ray intensity as a function of the scattering vector *s* is presented in a log–log coordinates for s = 0.007 - 0.170 $Å^{-1}$ (Fig. 2 a-c). Scattering vector is calculated as:

$$s = \frac{4\pi}{\lambda} sin\,\theta, \qquad (1)$$

where 2θ is a scattering angle.

The average slope of scattering data depends on the fractal dimension of the scattering system and allows calculating the size distribution of the scattering centers in the approximation $I(s) \sim s^{-n}$, where n = 2 for a perfectly smooth surface, 2 < n < 3 for a surface fractal, 3 < n < 4 for a highly folded or curved surfaces, n = 4 is characteristic of spherical interfaces and n > 4 corresponds to scattering on the rough surfaces.

The form of scattering curve for rGO sample is typical for polydisperse plate-like particles in the presence of large scatterers and is a result of scattering by surfaces of graphene packages. The power law dependency with n=3.58 was observed for small scattering vectors s (low-s Guinier region). Surface-fractal dimension D_s can be calculated as 6−n in this case. The lowest power-law exponent n = 1.9 was obtained at intermediate region of s (Fig.2 a) that determines mass-fractal dimension D_m. The radii of gyration (R_g) of the scattering objects were calculated using Guinier plot (Fig.2 b) and the slope $R_g^2/3$ of ln*I* vs s^2 dependencies. There are three characteristic sizes of the gyration radius of scattering objects for rGO – 21, 30 and 250 Å. We can make a conclusion that rGO particles form aggregates with a mass fractal dimension of 2.42 which are formed by plate-like particles. The average agglomerates size in spherical approach can be determined from the radius of gyration R_g obtained according to [13]:

$$d = 2\sqrt{\frac{5}{3}}R_g \qquad (2)$$

The obtained value of 65±15 nm corresponds to SEM data. The gyration radii of primary rGO particles were obtained using the intermediate-s Guinier approximation and $\ln(I_s)$ vs s plotting (Fig.2c). It is known that for cylinder of length L and radius R under these conditions

$$I(s) = \frac{I(0)}{s}\exp\left[-\frac{s^2 R_g^2}{2}\right], \qquad (3)$$

where $R_g^2 = R^2/2$. Assuming L << R we can estimate two mean primary sizes of plate-like particles – 5.2±0.4 and 5.7±0.4 nm. This result correlates with the normalized pair distance distribution functions F(d) obtained using GNOM software [14] for rGO sample that has two-mode distribution with the most probable particle size of 4.2 and 7.6 nm (Fig. 2 d). We can estimate the ratio between these two fraction content as 45:55. There is a weak Guinier plateau on the scattering curve of NIS sample in low *s* when scattered intensity is low dependent on s and is determined by scattering on the single particles. Power-law exponent n in this case is about 5.6 that can be explained by redistribution of electron density profile gradually in the superficial layers of the particle or between different phases [15]. Average sizes of agglomerates are about 62 nm when average sizes of primary particles are about 10 nm. These values differ from crystallite size obtained on the base of XRD data analysis and can be explained by polydispersity of NIS sample. This assumption is confirmed by declining character of Kratky plot ($s^2I(s)$ vs *s*) for this sample. The particle distribution function for NIS sample is close to symmetrical with maximum at about 50 nm. It can be divided into two components with most probable diameter of agglomerates about 42 and 55 nm with fraction ratio 40:60 (Fig. 2 e).

The most probable size of agglomerates for NIS /rGO composite materials is about 60 nm. Average size of primary particles is close for rGO and NIS /rGO samples that corresponds to main role of carbon component in X-ray scattering on non-crystalline domain in a multiphase system. Normalized pair distance distribution function for composite material is complex and can be optimally fitted as a superposition of at least four component correspond to fractions with most probable sizes of particle of about 4, 8, 16 and 35 nm (Fig. 2 f).

The room temperature Mossbauer spectra of NIS sample consist of a magnetically split sextet structure with broadened lines typical for ferrimagnetic spinels and a central superparamagnetic part (Fig. 3 a). The optimal fitting of the experimental data was obtained using 4 magnetic sextets and 2 superparamagnetic doublets (Table 1).

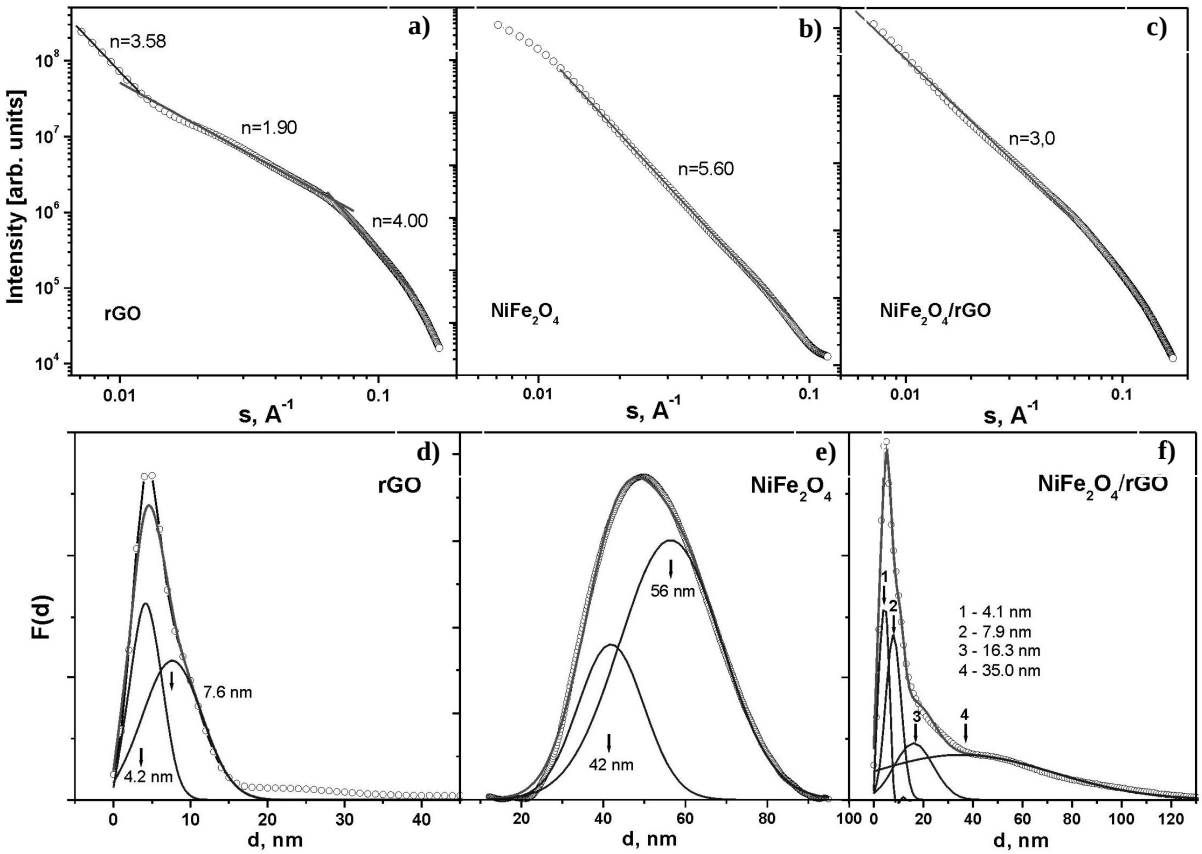

Fig. 2. Scattering profiles and normalized pair distance distribution functions F(d) with most probable particle sizes computed using GNOM for rGO, NIS and NIS / rGO samples

The identification of spectra components corresponds to fourfold and sixfold coordination of Fe ions was performed using isomeric shift (IS) values analysis. It is known that the increasing of covalency Fe-O chemical bonds for octahedrally coordinated Fe^{3+} due to shielding reducing and s-electron density enlarging results in IS decreasing [16]. In our case IS values for two spectra components with highest hyperfine fields (HF) are very close (about 0.36-0.37 mm / s) and about 30 % higher compared to IS for another two components with smaller HFs.

Thereby two pairs of components with bigger and smaller HF values correspond to Fe^{3+} ions located in tetrahedral and octahedral sites, respectively. Quadrupole splitting (QS) for all magnetic sextet components are close to 0, that corresponds to spherical symmetry of Fe^{3+} ions close surrounding typical for cubic spinel structure. The increasing of QS values for doublets components is caused by distortion of crystalline electric fields symmetry for ultrafine NIS particles. Bulk nickel ferrite $NiFe_2O_4$ is a typical inverse spinel with Ni^{2+} ions on octahedral interstitial positions of face centered cubic lattice formed by O^{2-} ions and Fe^{3+} ions distributed on tetrahedral and octahedral sites. At the same time the presence of Ni^{2+} ions in the tetrahedral positions was observed for $NiFe_2O_4$ nanoparticles with average sizes less than 10 nm [17, 18]. In this case mixed non-stoichiometry spinel structure will be formed with random occupancy of the octahedral and tetrahedral sites by Fe^{3+} and Ni^{2+} ions. According to XRFA data obtained sample can be described as: $Ni_{1.27}Fe_{1.73}O_{4-\delta}$. It is known that the ratio of Fe^{3+} molar contents in A- and B-sites determined the ratio of relative intensities of correspond spectra components S_A and S_B:

$$\frac{S_A}{S_B} = \frac{f_A}{f_B} \times \frac{[Fe_A^{3+}]}{[Fe_B^{3+}]} [16], \quad (4)$$

where f_A / f_B =0.94 – the ratio of the recoilless fractions for octahedrally and tetrahedrally coordinated Fe^{3+} ions [40]. It is clear that Fe^{3+} ions located in superparamagnetic particles have the same probability belong to A and B sublattices. In our case $\frac{[Fe_A^{3+}]}{[Fe_B^{3+}]} = 0.65$ that allows calculating Fe^{3+} ions distribution between sublattices: $(Ni_{0.32}Fe_{0.68})[Ni_{0.95}Fe_{1.05}]O_{4-\delta}$, where δ is oxygen non-stoichiometry parameter. The presence of Ni^{2+} ions at the tetrahedral sites will result in varies the number of Fe^{3+} ions nearest neighbors in both sublattices. The probability of Fe^{3+} ions finding with different number of iron ions in second coordination sphere will determine the intensity and other parameters of the components of Mossbauer spectra formed as a result of resonant absorption by nucleus of these ions.

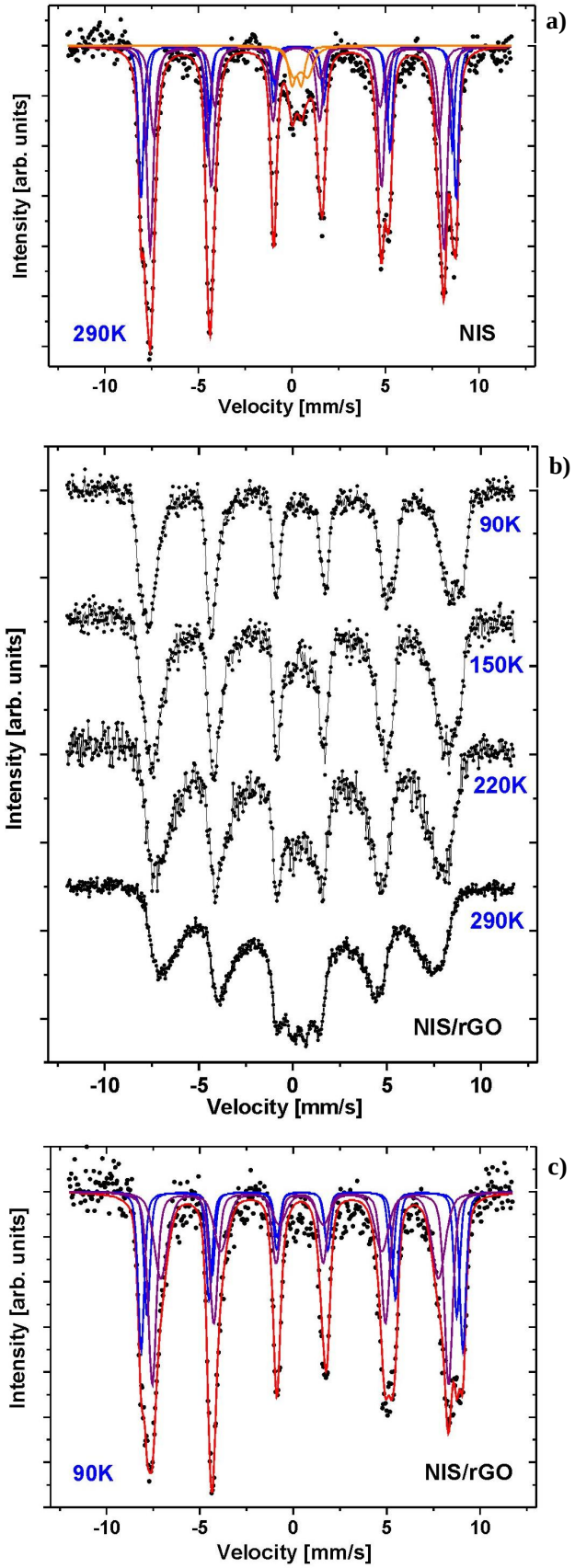

Fig. 3. Mossbauer spectra of NIS (a), NIS / rGO samples obtained at different temperatures (b) and NIS / rGO samples at 90 K (c).

TABLE I. Fitting parameters of the Mössbauer spectra of $NiFe_2O_4$ and NIS / rGO samples

Site	Is, mm/s	Qs, mm/s	H, kOe	S, %	G, mm/s
NIS, T=295 K					
A1	0.36±0.01	-0.01±0.01	523±1	21.3	0.32±0.04
A2	0.37±0.01	0.03±0.01	509±2	13.6	0.30±0.07
B1	0.26±0.01	0.04±0.01	488±2	38.0	0.42±0.05
B2	0.26±0.01	-0.08±0.02	473±1	19.2	0.49±0.04
D1	0.46±0.01	0.76±0.02	–	4.3	0.72±0.06
D2	0.25±0.02	0.50±0.03	–	3.4	0.44±0.08
NIS / rGO, T=90 K					
A1	0.48±0.02	-0.02±0.01	535±2	22.1	0.40±0.04
A2	0.46±0.03	0.01±0.02	515±3	16.6	0.38±0.07
B1	0.36±0.02	0.04±0.02	493±3	35.6	0.53±0.05
B2	0.38±0.03	-0.08±0.03	462±2	25.8	0.86±0.04

This probability $P_z^{(n)}$ can be calculated using binomial distribution as:

$$P_z^{(n)} = \frac{z!}{n!(z-n)!} k^{(z-n)} (1-k)^n, \quad (5)$$

where z is a number of cations in close surrounding of Fe^{3+} ions in A- and B crystallographic positions, n is number of magnetic neighbors of Fe^{3+} ions ($0 \le n \le z$), k is a relative amount of Ni^{2+} at opposite sublattice. Each Fe^{3+} ions located on tetrahedral and octahedral sites has 8 and 6 cation positions in close surrounding [19]. Using data about Fe^{3+} and Ni^{2+} ions distribution the number of crystallography non-equivalent position of Fe^{3+} ions was calculated that allows evaluating independently the number of component that is needed for Mossbauer spectra description (Fig. 4).

The calculated probability for A sites can be divided into two groups – $0 \le n \le 5$ and $6 \le n \le 8$ that corresponds to A1 and A2 spectra component (Fig. 4 a). Predicted from binomial distribution integral intensity of A1 and A2 are 19.5 and 19.8 %, respectively. Similar calculation for B-sublattice gives values of B1 and B2 component as 37.0 and 27.7 % (Fig. 4 b). The obtained values are in good agreement with the experimental ones (Table 1).

Bulk nickel iron ferrite $NiFe_2O_4$ is a collinear ferrimagnetic material with antiparallel orientation of the magnetizations of tetrahedral and octahedral sublattices. Thereby the reduction of crystallite size leads to the noncollinear magnetic structure formation due to spin canting in superficial layers of particles [20]. The main reason of this magnetic disordering is rearrangement of lower coordinated ions in near-surface regions of particles which leads to disturbing and destruction of Fe_A-O-Fe_B exchange interaction. As a result the transition of some particles to spin-glass state and further to superparamagnetic state is possible. The probability of these transitions depends on the particle size, constant of magnetic anisotropy and temperature [21]. The average canting angle θ was calculated using Mössbauer data as :

$$\theta = 90^{o} - \arcsin\left\{\left[3\left(I_{2,5}/I_{1,6}\right)/2\right]/\left[1+3\left(I_{2,5}/I_{1,6}\right)/4\right]\right\}^{1/2} \quad (6)$$

where $I_{1.5}$ and $I_{1,6}$ are the integral intensity of separate lines number 2 or 5 and 1 or 6 of magnetic sextet component of Mossbauer spectra. The average canting angle for NIS sample was obtained as $(35.7\pm1.2)^{o}$.

The Mossbauer spectra of NIS / rGO composite obtained at different temperatures presented in Fig. 3 b. Room-temperature Mossbauer spectra of NIS / rGO demonstrate broadening of spectral components and partically disappearance of magnetic hyperfine interactions. These effects can be explained by core-shell magnetic structure of spinel nanoparticles where near-surface crystall disodering cause the spin canting of sublattices for intermediate sizes at fixed temperature with extension of spin-glasslike surface layer and transition with particle sizes decreasing to state of monodomain cluster with fluctuated magnetic moments (classical theory of superparamagnetic relaxation). The relaxation time τ_r of particle magnetic moment fluctuation is calculated as:

$$\tau_r = \tau_0 \exp\left(\frac{KV}{kT}\right), \quad (7)$$

where $\tau_0 \approx 10^{-9}$-10^{-11} s, V– particle volume, K– constant of magnetic anisotropy, T– temperature. For a particle with the certain values K and V the transition to superparamagnetic state occurs at the blocking temperature T_B . It was determined that superparamagnetic relaxation disappears at about 90 K. That means the time of magnetic moment relaxation τ_r for particles of all sizes satisfy the condition $\tau_r < \tau_{lf}$ where τ_{lf} =141.8 ns for ^{57}Fe is a lifetime of absorbing nucleus excited state. According to [22] constant of magnetic anisotropy of $NiFe_2O_4$ spinels at 90 K is about (5-6)· 10^5 J / m^3.

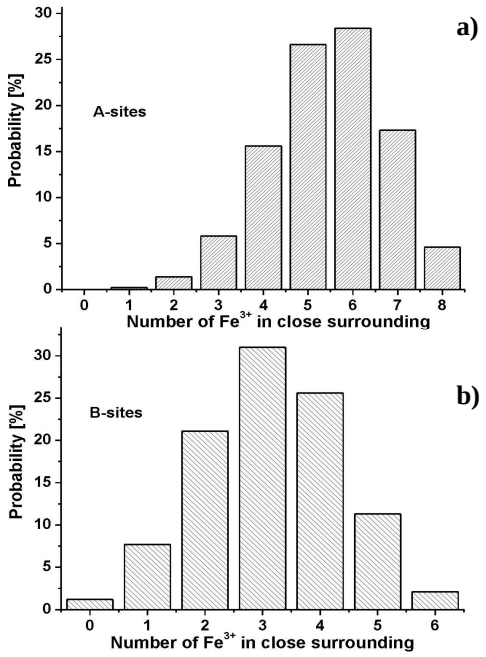

Fig. 4. The probabilities of different numbers of iron cations in the close surrounding of Fe^{3+} ions in A- (a) and B-sites (b) of $(Ni_{0.32}Fe_{0.68})[Ni_{0.95}Fe_{1.05}]O_{4-\delta}$ spinel structure

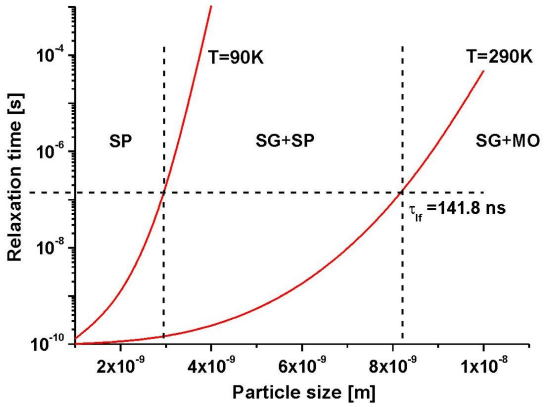

Fig.5. The relaxation time of magnetic moment for NIS monodomain particles in NIS / rGO composite material as a function of crystallite size

The calculated dependency of relaxation time as a function of particle size at different values of temperature is shown in Fig. 5. Calculation was performed for $\tau_0 = 10^{-10}$s , K values were $6\cdot10^5$ and $1\cdot10^5$ J / m^3 at 90 and 290 K, respectivelly. The lower threshold of NIS particle size for NIS / rGO sample was about 3 nm. At room temperature for particles with the sizes in a range of 3 - 8 nm the transition from spin glass (SG) to superparamagnetism (SP) states were observed. Particles (crystallites) with the sizes more than 9 nm are in magnetic ordered state with spin canting surface effects. Mossbauer spectra of NIS / rGO system at 88 K were analyzed. The optimal fitting results were achieved for 4 magnetic sextets (Table 1). The increased values of IS for tetrahedral sites were observed in this case too. QS values of Mossbauer spectra component for NIS and NIS / rGO are very close. Spinel composition for NIS / rGO material was determined by XRFA methods as $Ni_{1.27}Fe_{1.73}O_{4-\delta}$. Calculated cation distrubution for NIS / rGO can be written as $(Ni_{0.27}Fe_{0.73})[Ni_{0.91}Fe_{1.09}]O_{4-\delta}$. The average canting angle for NIS / rGO is about $(35.9\pm1.3)^{o}$.

IV. CONCLUSIONS

Ultrafine nickel iron spinel (NIS) and NIS /reduced graphene oxide (rGO) nanocomposites were synthesized via a hydrothermal method. The average crystallite sizes (XRD data) for NIS and NIS /rGO are 26 and about 8 – 9 nm, respectively. It was found that the plate-like particles rGO particles with most probable average sizes 4.2 and 7.6 nm form aggregates with a mass fractal dimension of 2.42 and average sizes 65 nm**.** The agglomerates for NIS /rGO composite materials with average size about 60 nm are formed by the particles with most probable sizes of 4.1, 7.9, 16.3, 35.0 nm. It was determined that NIS / rGO have mixed structure $(Ni_{0.27}Fe_{0.73})[Ni_{0.91}Fe_{1.09}]O_{4-\delta}$. The Mössbauer spectroscopy allows observing the transitions between magnetic ordered, spin glass like and superparamagnetic state of ultrafine nickel ferrite. It was found that NIS particles with the sizes of 3 - 8 nm in NIS /rGO composite have both spin glass and superparamagnetic properties. The average spin canting angles both for NIS and NIS / rGO samples are close to 36^{o}. The results show that NIS / rGO nanocomposites are promising magnetic porous material.

V. REFERENCES

1. V.Šepelák, I. Bergmann, A. Feldhoff, P. Heitjans, F. Krumeich, D. Menzel, K. D. Becker, “Nanocrystalline nickel ferrite, $NiFe_2O_4$: mechanosynthesis, nonequilibrium cation distribution, canted spin arrangement, and magnetic behavior”.J Phys Chem C, vol. 111, pp. 5026-5033, September 2007.
2. Pedro Tartaj, Marıa del Puerto Morales, Sabino Veintemillas-Verdaguer, Teresita Gonzalez-Carre and Carlos J Serna, "The preparation of magnetic nanoparticles for applications in biomedicine", J Phys D: Appl Phys, Madrid, vol. 36, R182-R197, June 2003.
3. Sharifi Ibrahim, H. Shokrollahi, and S. Amiri, "Ferrite-based magnetic nanofluids used in hyperthermia applications", J Magn Magn Mater vol. 324 pp. 903-915, 2012.
4. Polshettiwar, Vivek, and S. Varma Rajender, "Green chemistry by nano-catalysis", Green Chemistry vol. 12, pp. 743-754, 2010.
5. Reddy, D. Harikishore Kumar, and Yeoung-Sang Yun, "Spinel ferrite magnetic adsorbents: alternative future materials for water purification?." Coord Chem Rev, vol. 315, pp. 90-111, 2016.
6. Hongxiao Zhao, Zhi Zheng, Ka Wai Wong, Shumin Wang, Baojun Huang, Dapeng Li, "Fabrication and electrochemical performance of nickel ferrite nanoparticles as anode material in lithium ion batteries", Electrochem Commun vol. 9, pp. 2606-2610, 2007.
7. P. T. A. Santos, A. C. F. M. Costa, R. H. G. A. Kiminami, H. M. C. Andrade, H. L. Lira, L. Gama, "Synthesis of a $NiFe_2O_4$ catalyst for the preferential oxidation of carbon monoxide (PROX)", Journal of Alloys and Compounds, vol. 483, pp. 399-401, 2009.
8. Fengmin Wu, Xiaowei Wang, Mei Li, Hang Xu, "A high capacity $NiFe_2O_4$/RGO nanocomposites as superior anode materials for sodium-ion batteries", Ceramics International, vol.42, pp. 16666-16670, 2016.
9. K. Hareesh, B. Shateesh, R.P. Joshi, S.S. Dahiwale, V.N. Bhoraskar , S.K. Haram, S.D. Dhole,. "PEDOT: PSS wrapped $NiFe_2O_4$/rGO tertiary nanocomposite for the super-capacitor applications" Electrochimica Acta, vol. 201, pp. 106-116, 2016.
10. Chen Li, Xia Wang, Shandong Li, Qiang Li, Jie Xu, Xiaomin Liu, Changkun Liu, Yuanhong Xu, Jingquan Liu, Hongliang Li, Peizhi Guo, Xiu Song Zha, "Optimization of $NiFe_2O_4$/rGO composite electrode for lithium-ion batteries", Applied Surface Science, vol. 416, pp. 308-317, 2017.
11. J. Chen, Y. Li, L. Huang, C. Li, G. Shi, “High-yield preparation of graphene oxide from small graphite flakes via an improved Hummers method with a simple purification process”, Carbon,vol. 81, pp. 826-834, 2015.
12. L. Stobinski, B. Lesiak, A. Malolepszy, M. Mazurkiewicz, B. Mierzwa, J. Zemek, I. Bieloshapka, “Graphene oxide and reduced graphene oxide studied by the XRD, TEM and electron spectroscopy methods”, J Electron Spectrosc Relat Phenom, vol. 195, pp. 145-154, 2014.
13. A. Guinier, G. Fournet, “Small Angle Scattering of X rays”, John Wiley & Sons, New York, 1955.
14. A. V. Semenyuk, D. I. Svergun, "GNOM–a program package for small-angle scattering data processing", J Appl Crystallogr, vol. 24, pp. 537-540, 1991.
15. X. Guo, K. Gao, A. Gutsche, M. Seipenbusch, H. Nirschl, “Combined small-and wide-angle X-ray scattering studies on oxide-supported Pt nanoparticles prepared by a CVS and CVD process”, Powder Technology, vol. 272, pp. 23-33, 2015.
16. Jacob John, M. Abdul Khadar. "Investigation of mixed spinel structure of nanostructured nickel ferrite." J Appl Phys, vol. 107, pp. 114310 (1)- 114310 (10), 2010
17. A. Ahlawat, V.G. Sathe, V.R. Reddy, A. Gupta, “Mössbauer, Raman and X-ray diffraction studies of superparamagnetic NiFe2O4 nanoparticles prepared by solgel auto-combustion method”, J. Magn. Magn. Mater., vol. 323, pp. 2049–2054, 2011
18. C. N. Chinnasamy, A. Narayanasamy, N. Ponpandian, R.J. Joseyphus, J. Jeyadevan, K. Tohji, K. Chattopadhyay, “Grain size effect on the Néel temperature and magnetic properties of nanocrystalline $NiFe_2O_4$ spinel”, J. Magn. Magn. Mater., vol. 23, pp. 281–287, 2002.
19. M. V. Ushakov, B. Senthilkumar, R. K. Selvan, I. Felner, M. I. Oshtrakh, “Mössbauer spectroscopy of $NiFe_2O_4$ nanoparticles: The effect of Ni^{2+} in the Fe^{3+} local microenvironment in both tetrahedral and octahedral sites”, Materials Chemistry and Physics,vol. 202, pp. 159-168, 2017
20. S. Morup, E. Brok, C. Frandsen, “Spin structures in magnetic nanoparticles”, Journal of Nanomaterials, 2013.
21. V. Kotsyubynsky, V. Moklyak, A. Hrubiak, “Synthesis and Mossbauer studies of mesoporous γ-Fe_2O_3”, Materials Science-Poland, vol. 32, pp. 481-486, 2014.
22. T. S. Karpova, V. G. Vasil’ev, E. V. Vladimirova, A. P. Nosov, “Synthesis of ferrite spinel $NiFe_2O_4$ by thermal hydrolysis and its magnetic properties”, Inorganic Materials: Applied Research, vol. 3, pp. 107-11, 2012